Journal of Magnetism and Magnetic Materials 487 (2019) 165335

Contents lists available at ScienceDirect

Journal of Magnetism and Magnetic Materials

journal homepage: www.elsevier.com/locate/jmmm

Research articles

Effect of colossal magnetoresistance material $La_{0.67}Ca_{0.33}MnO_3$ on superconducting properties of $YBa_2Cu_3O_{7-\delta}$ thin films

T.B. Hjelmeland[a], C. Bazioti[a], A.E. Gunnæs[a], Y. Volkov[b], P. Mikheenko[a,*]

[a] Department of Physics, University of Oslo, P.O. Box 1048, Blindern, 0316 Oslo, Norway
[b] Faculty of Physics, Taras Shevchenko National University of Kyiv, Hlushkova Avenue 4, 03127 Kyiv, Ukraine

ARTICLE INFO

Keywords:
High temperature superconductor
Colossal magnetoresistance material
Spin injection
Nano-magnetism
Graphene

ABSTRACT

By specific design of the sample, in which $SrTiO_3$ substrate is fully covered by a thin layer of the colossal magnetoresistive material $La_{0.67}Ca_{0.33}MnO_3$ (LCMO) and the latter is partially covered by high-temperature superconductor $YBa_2Cu_3O_{7-\delta}$ (YBCO), and by using multiple current and voltage contacts, direct evidence of the strong effect of LCMO on YBCO is obtained. It is found that LCMO strongly influences not only superconducting, but also normal state of YBCO, and it is argued that this is a consequence of the spin injection from the former to the latter. The effect of the deposition conditions and crystal orientation of YBCO layer on this effect is clarified. A surprising peak in the temperature dependence of resistance seen in ex-situ *ab*-plane oriented sample is explained as a combination of two effects: influence of spin-polarized electrons on superconductor below its critical temperature and the interface-controlled shift of Curie temperature of LCMO to low temperatures. Considering expected use of LCMO and YBCO in composite quantum computation circuits, their combination with another advanced quantum material, graphene, is explored.

1. Introduction

With advance of superconducting quantum computing [1], there is a renewed interest in high-temperature superconductors in combination with spin-polarized materials [2], which is stimulated by the attempts to confine quantum processing on nanometer scale, making computers more compact, and extend their operation to higher temperatures [3]. Graphene is another important material, which demonstrates quantum behavior even at room temperature [4]. Merging spin-polarized materials, superconductors and graphene might lead to novel quantum devices with enhanced performance and functionality.

Two particular materials: spin-polarized $La_{0.67}Ca_{0.33}MnO_3$ (LCMO) and high-temperature superconductor $YBa_2Cu_3O_{7-\delta}$ (YBCO) are of special interest [5]. They have similar crystal lattice structure and can be grown together epitaxially. There are multiple investigations of these compounds and their effect on each other [5–8].

The properties of LCMO are described in references [9–12] with emphasis on colossal magnetoresistive behavior and spin polarization. The idea of merging spin-polarized materials with high temperature superconductors have been explored by many researchers during the last decades [8,13–16]. In this combination of materials, the half-metallic LCMO is responsible for the suppression of both the proximity effect and the Andreev reflection [14,17], which weakens the superconducting properties near the LCMO-YBCO interface. Such an influence opens the possibility to utilize LCMO for controlling superconductivity in thin layers of YBCO by means of spin-polarized injections of quasiparticles. This is also applicable to other systems combining superconducting and half-metallic materials and reflects the fact that strong exchange energy is able to brake Cooper pairs [14].

The systems, which merge spin-polarized materials with superconductors, reveal interesting properties like enhancement of spin lifetime in superconductors by several orders of magnitude, as compared to its lifetime in ferromagnets [2,18,19]. This is especially relevant when the energy of the injected quasiparticles is close to the energy of the superconducting gap. Such a behavior leads to a charge-spin separation [20,21], a reduction of quasiparticles velocities, an increase of time between subsequent scattering events and thus to increase of the spin lifetime in the superconductor [2]. It is envisaged that in such systems electrons could be transported without energy dissipation while conserving the polarization of their spin [2,18–20].

The idea of merging superconducting and spin-polarized materials with graphene is a novel one inspired by the quantum properties of graphene at high temperatures. High conductivity of graphene is an additional useful property that could further reduce dissipation in the system.

Due to the complexity of the materials and their combinations,

* Corresponding author.
E-mail address: pavlo.mikheenko@fys.uio.no (P. Mikheenko).

https://doi.org/10.1016/j.jmmm.2019.165335
Received 3 September 2018; Received in revised form 27 March 2019; Accepted 20 May 2019
Available online 21 May 2019

simple experiments revealing important features of the interaction between superconductors, spin-polarized materials and graphene are rare. This paper demonstrates such experiments performed using multi-contact configurations on specially prepared bilayers.

LCMO and YBCO are delicate compounds. Small changes in their chemical composition, especially oxygen content, presence of impurities or diffusion of elements through the interface can produce unexpected effects, like appearance of stripy magnetic structure and resistance peak below the critical temperature of superconductor found in [22]. Another important issue is the orientation of the YBCO relative to the LCMO in the bilayers. It is now confirmed that in the sample investigated in [22], YBCO is oriented with the *ab*-planes perpendicular to the plane of the film. Important consequence of this is the shift of Curie temperature (T_{Curie}) of LCMO to a lower temperature, which is close to the critical temperature (T_c) of YBCO [22]. Following this, the paper discusses the effect of YBCO orientation on the properties of the interface between YBCO and LCMO explaining the origin of the resistance peak. The combination of LCMO and YBCO with graphene is also explored using multiple contacts on the bilayers.

2. Experimental

The main LCMO-YBCO bilayer investigated in this work was epitaxially grown by pulsed laser deposition on a $SrTiO_3$ (STO) substrate. First, the 5x10-mm^2 substrate was fully covered by a 100-nm thick layer of LCMO. After that, not removing sample from the chamber and using a mask, about half of the LCMO surface was covered by a 100-nm thick layer of YBCO, as illustrated in Fig. 1. Both YBCO and LCMO layers were oriented with c-axis perpendicular to the plane of the film, and the sample is referred to as *in-situ* YBCO/LCMO.

Another investigated sample is the LCMO/YBCO bilayer previously described in [22]. The YBCO film was grown with resulting *ab*-plane orientation (*c*-axis in plane of the sample), as it is confirmed in the current study. The sample was removed from the chamber after the deposition of YBCO in order to investigate its properties, after which it was cleaned and returned to the chamber for the deposition of LCMO. The sample is referred to as *ex-situ* LCMO/YBCO.

In the experiments with graphene, the latter was used in the available form of water solution with graphene nano-plates of the in-plane sizes from fractions of micron to few microns (Sigma-Aldrich, graphene nanoplatelets 1 mg/mL). A drop of the solution was applied to a region of interest on YBCO or LCMO and was left drying while recording resistance of the sample. Such solution was already found useful in investigations of superconductivity in biological samples [23,24], and it is interesting to explore it in the combination with solid-state materials.

Electrical measurements on the *in-situ* sample were done using several indium contacts pressed to its surface as illustrated in Fig. 1. Four of the contacts were on the YBCO and two on LCMO surface. These contacts allow for a variety of measurements depending on which of them are used for passing current and which for measuring voltage. For example, if current is flowing from I_1 to I_3, charge carriers are transferred from LCMO to YBCO. On the other hand, for I_1 and I_2, charge carriers are mainly confined to the YBCO layer. At a defined current path, a variety of measurements could be done using different potential contacts.

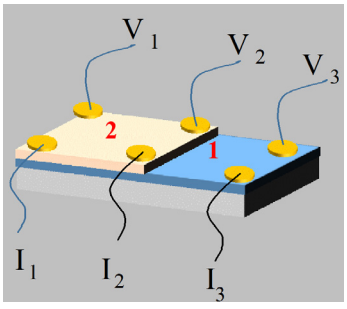

Fig. 1. Schematic illustration of the *in-situ* sample with 100-nm thick layers of LCMO (1) and YBCO (2) on a STO substrate. Six contacts are attached to the sample. Three of them are used for passing current (I_{1-3}) and three for measuring voltage (V_{1-3}).

Before attaching indium contacts, the samples were investigated (see details for the ex-situ sample in [22]) by magneto-optical imaging and scanning electron microscopy. Here the focus is on the electrical transport measurements performed with a constant-voltage load technique. The paper mainly deals with temperature dependence of the resistance in different parts of the sample.

The sample shown in Fig. 1 with the attached wires was mounted on an insulating plate connected to a rod, whose temperature was changed by lowering it in, or retracting from a liquid-nitrogen or liquid-helium dewar. The temperature was measured by a sensor attached to the plate holding the sample. Electrical measurements were done sufficiently slow to avoid appearance of hysteresis in resistance at the increase and decrease of temperature. The absence of the hysteresis is treated as an argument that heating in the samples is small and unlikely to be the dominant reason for the effects described in this paper.

The constant-voltage load in electrical measurements is a simple approach that does not require adjustment of current due to the change of resistance when varying the temperature. Its disadvantage is that the current does not remain constant during the temperature scans. However, monitoring it allows obtaining additional information, in particular about the quality of the contacts.

After electrical measurements, the samples were investigated in a transmission electron microscope (TEM). The TEM samples preparation for the cross-sectional observations was performed by mechanical grinding, using the conventional tripod wedge polishing protocol in an Allied Multiprep setup. The final thinning of the specimens was done by Ar+ ion milling in a Gatan PIPS II system and, finally, the samples were plasma cleaned using a Fichione Model 1020 plasma system in order to minimize carbon surface contamination. STEM (Scanning TEM) observations were performed in a probed-corrected FEI Titan G2 60–300 microscope operated at 300 kV.

3. Results and discussion

Fig. 2 shows a low-magnification High-Angle Annular Dark-Field (HAADF)-STEM image, presenting the overall morphology of the YBCO/LCMO/STO heterostructure. Both LCMO and YBCO layers are dense, and the interface between them is sharp. However, grain boundaries are present in YBCO. One of them is marked by the vertical white arrow.

The presence of grain boundaries and associated with them polycrystallinity is also seen in electron diffraction. While selected-area electron diffraction (SAED) patterns acquired from the LCMO layer

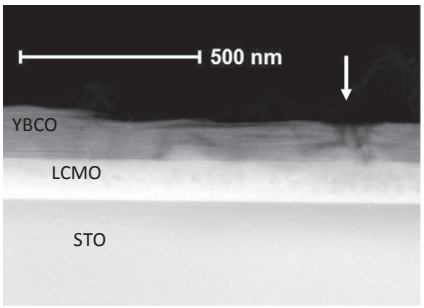

Fig. 2. HAADF-STEM image, illustrating the overall morphology of the YBCO/LCMO/STO heterostructure. A grain boundary in the YBCO film is indicated by white arrow.

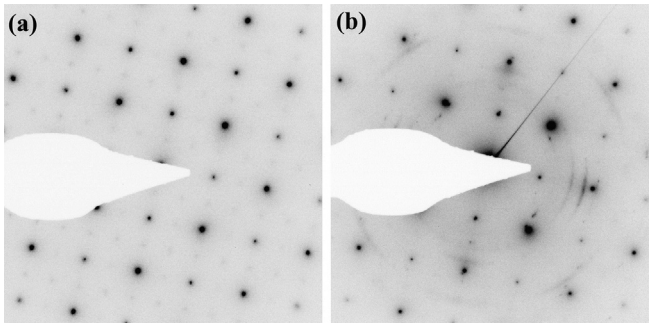

Fig. 3. SAED patterns from (a) LCMO and (b) YBCO (with admixture of LCMO). A single-domain LCMO structure is revealed (clear visible dots), while the YBCO film shows slightly-misoriented polycrystallinity (arc-shaped segments).

(Fig. 3(a)) shows its single-crystallinity (clear visible dots), YBCO region (Fig. 3(b)) gives arc-shaped intensities typical for slightly misoriented polycrystalline structure.

Despite the polycrystalline character of YBCO, at the first stages of growth, it achieves good heteroepitaxial relationship with the LCMO forming single-domain film. Fig. 4 shows a high-resolution HAADF-STEM image taken over the cross section of the YBCO/LCMO interfacial area. The color labels indicate different elements as identified from the HAADF-STEM image, in which the contrast is sensitive to the atomic number. Smooth interface at the atomic level was revealed (indicated by the horizontal white arrow) showing the high epitaxial quality of the heterostructure. Such a high quality opens possibilities for making nano-devices based on the bilayers.

Following the sequence of layers, local stoichiometric variations were observed in YBCO due to intergrowths of extra CuO chains. The occurrence of double CuO chains (indicated by the blue arrow in Fig. 4(a) and shown in detail in Fig. 4(b)), was compensated by missing CuO chains elsewhere else in the film (green arrow). These variations generate a non-planar growth as demonstrated by the 'waviness' of the YBCO layers. It has been previously reported that extra double CuO chains can account for the reduced critical temperature of the bilayer thin film [25].

In contrast to the *in-situ* YBCO/LCMO/STO sample, in which the

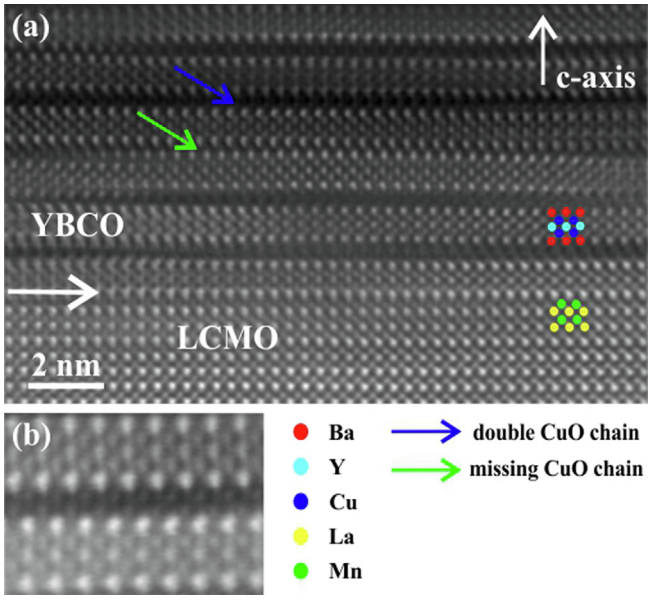

Fig. 4. High-resolution HAADF-STEM image of the YBCO/LCMO interfacial area. An atomically sharp interface is evident. The YBCO structure reveals intergrowths of double CuO chains compensated by missing CuO chains elsewhere else in the film.

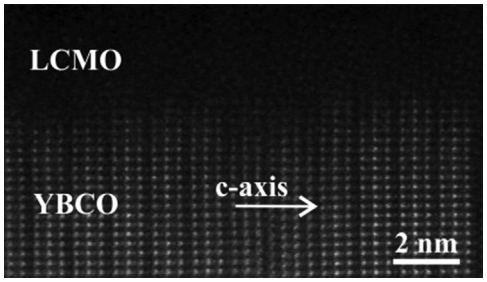

Fig. 5. A high-resolution HAADF-STEM image of the LCMO/YBCO interface of the *ex-situ* sample. YBCO is *ab*-plane oriented and LCMO is strongly disordered close to the interface.

YBCO was found to have a polycrystalline texture with *c*-axis growth, the LCMO/YBCO/STO *ex-situ* sample demonstrates a single crystalline YBCO with an *ab*-plane orientation shown in Fig. 5. However, its LCMO/YBCO interface, which is important for spin injection, appears to be not atomically sharp. Few LCMO layers left above YBCO after the polishing seem to be strongly disordered, which could be the reason behind specific electrical and magnetic properties of LCMO found in [22]. These properties will be discussed after describing electrical behavior of the *in-situ* sample.

The temperature dependence of the resistance (R(T)) of the *in-situ* sample with current flowing from I_1 to I_3 and voltage measured between V_1 and V_3 (see Fig. 1) is shown in Fig. 6. It was recorded at a fixed voltage load of 6 V. Both magnetic and superconducting transitions in LCMO (main plot) and YBCO (inset), respectively, are clearly visible. The magnetic transition is seen as accompanying it sharp decrease in the resistance at the Curie temperature (T_{Curie}) of about 250 K, which is typical value for the single-crystalline LCMO [5–8]. The superconducting transition, which is shown in the magnified plot in the inset, takes place at the temperature of about 80 K. This is somewhat lower than T_c of optimally-doped YBCO and could be linked to the presence of CuO intergrowths [23]. Such low T_c could also indicate possible oxygen inter-diffusion between YBCO and LCMO, which is, again, typical for the growth of these compounds on top of each other without separating barrier between them. Below the superconducting transition, the resistance is not zero, because in this configuration there is a layer of normal LCMO connected in series with YBCO. The long tail below T_c comes from the overlap of R(T) curves of the superconducting and magnetic materials.

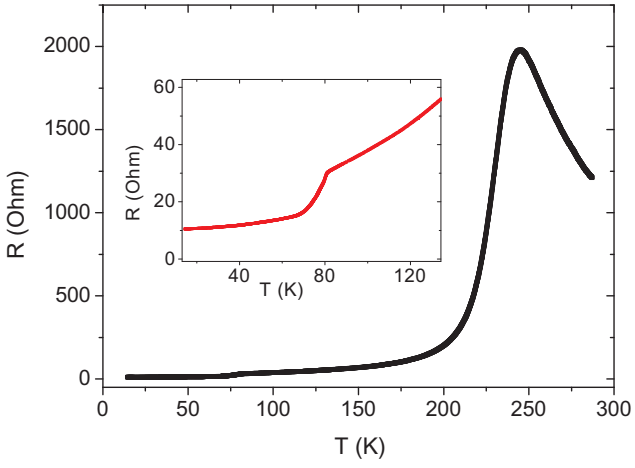

Fig. 6. Temperature dependence of resistance for the *in-situ* sample schematically shown in Fig. 1 with current flowing from I_1 to I_3 and voltage measured between V_1 and V_3. The curve was recorded at a fixed voltage load of 6 V. Inset shows magnified part of the curve around the superconducting transition of YBCO.

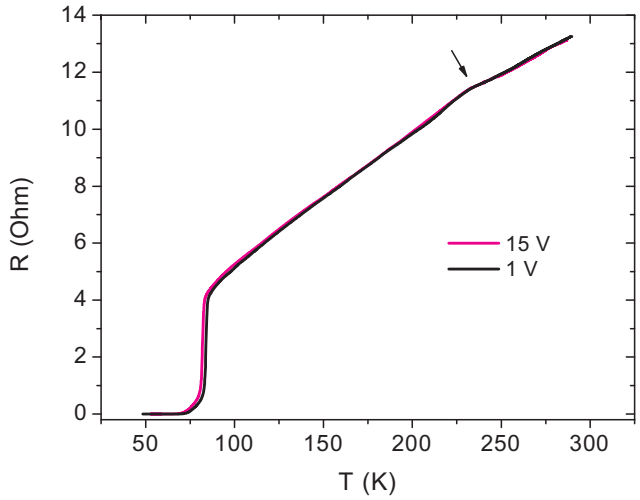

Fig. 7. Temperature dependence of resistance for the *in-situ* sample schematically shown in Fig. 1 with current flowing, as in Fig. 6, between contacts I_1 and I_3, but voltage measured between contacts V_1 and V_2. Two curves for the load voltages of 1 and 15 V are displayed.

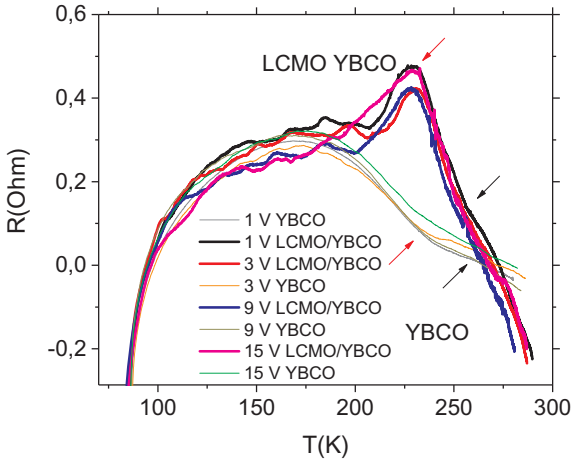

Fig. 8. Temperature dependence of resistance for the *in-situ* sample with current flowing between contacts I_1 and I_3 (bold lines) and between contacts I_1 and I_2 (thin lines). The voltage is measured between contacts V_1 and V_2 (see Fig. 1). A linear curve is subtracted from each set of data, both recorded at the same varied voltages, whose values are shown in the legend.

Several curves, similar to that shown in Fig. 6, were recorded at different voltage loads. They also register two transitions with minor systematic variations between them. At the constant voltage load, measurement current increases at both superconducting and magnetic transitions. Following this property, temperature dependence of current was used to accurately identify transitions, and check quality of the contacts. Overall behavior shows that contact resistance is not the dominant resistance in the circuit. Therefore, described effects are unlikely to be caused by the overheating, especially that expected from the current leads contacts. With all contacts of a high quality, the design in Fig. 1 allows to explore different parts of the sample at different paths for the current, which can either be confined to one of the materials or flow between different ones.

In Fig. 7, the temperature dependence of the resistance for the same sample as in Fig. 6 with current flowing between contacts I_1 and I_3, but with voltage measured between contacts V_1 and V_2, which are positioned directly on YBCO, is shown. Two curves for the voltage loads of 1 and 15 V are plotted to emphasize weak dependence of the resistance on the measurement current. The measured R(T) are in sharp contrast with that shown in Fig. 6. Since in this experiment, current mainly flows in YBCO, resistance shows a monotonous quasi-linear decrease with decreasing the temperature. Below the superconducting transition, the resistance is zero. This is a typical R(T) curve for a YBCO sample with one exception: there is a small, but distinctive anomaly at the Curie temperature of LCMO marked by a small arrow in Fig. 7.

The shape of the anomaly is counterintuitive. Since YBCO is on the top of the LCMO layer, one would expect a decrease in the resistance at T_{Curie}, at which resistance of LCMO suddenly drops with the decrease of the temperature. Instead, the resistance is increasing. It indicates that charge carriers have difficulties of overflowing from LCMO to YBCO at temperatures below T_{Curie}. It is natural to expect since all spins in LCMO have one preferential orientation below T_{Curie}.

One would expect a different outcome when current is not injected from the LCMO to YBCO, but simply flows between different parts of YBCO, for example, when it is passed between contacts I_1 and I_2. Indeed, in this case an increase in resistance does not take place. A comparison between these two cases is given in Fig. 8 for a set of load voltages shown in the legend in the inset. Bold curves are for the current flowing between I_1 and I_3, and the thin curves are for the current flowing between I_1 and I_2.

For a better comparison, a linear curve is subtracted from each set of data. Black arrows indicate the beginning of the spin polarization transition, while red arrows show the positions of a maximum or minimum in the resistance, which appear in the presence or absence of suggested spin injection, respectively. The curves at different voltages in Fig. 8 are shown to demonstrate the reproducibility of the results.

The same approach of changing position of the current leads, but keeping potential leads at the same location, i.e. injecting spin-polarized electrons or just passing current mainly in YBCO, can be used to demonstrate effect of spin-polarized LCMO on superconducting state of YBCO. Fig. 9 shows temperature dependence of the resistance of YBCO, measured between contacts V_1 and V_2, in the vicinity of superconducting transition.

In this experiment, current is passed through the contacts I_1 and I_3 (black curves), and I_1 and I_2 (red) at four voltage loads of 1, 3, 9 and 15 V. The black curves represent the case of current flow from LCMO to YBCO, while the red curves correspond to current mainly flowing in YBCO (some overflow of current to LCMO is still possible). It is clear that transfer of charge carriers from LCMO to YBCO strongly affects the superconducting transition, and its influence increases with the increase of the load voltage.

Blue curves in Fig. 9 are the difference curves between black and red ones. These curves show the additional resistance caused by the transfer of charge carriers from LCMO to YBCO. One can see that influence on transition is strongest just below T_c, where superconductivity is relatively weak. The blue peaks are added to the red curves giving the apparent shift in the superconducting transition. Such a behavior explains similar resistance peak observed in [22].

The sample in [22] was prepared *ex-situ*, i.e. deposition of LCMO above YBCO took place after removing the sample from the deposition chamber. Due to this and specific *ab*-plane orientation of superconductor, the T_{Curie} of LCMO was shifted to a temperature close to T_c of YBCO. With decreasing temperature, first, the superconducting transition takes place with a corresponding drop in the resistance at about 90 K. After that, spin-polarization in LCMO settles in forming the peak similar to that shown by blue curves in Fig. 9. It is important to note that such a peak can only be seen if T_{Curie} is close to T_c. Otherwise, effect of charge carriers flowing from LCMO to YBCO results in a gradual shift of resistance transition shown in Fig. 9.

To independently confirm the magnetic nature of the influence of current flowing from LCMO to YBCO, the current was stabilized, and the voltage was measured in a similar to investigated bilayer, while changing applied magnetic field along the magnetization loop of LCMO. The results of such an experiment are shown in Fig. 10.

The influence of magnetic field, which is aligning spins in LCMO is

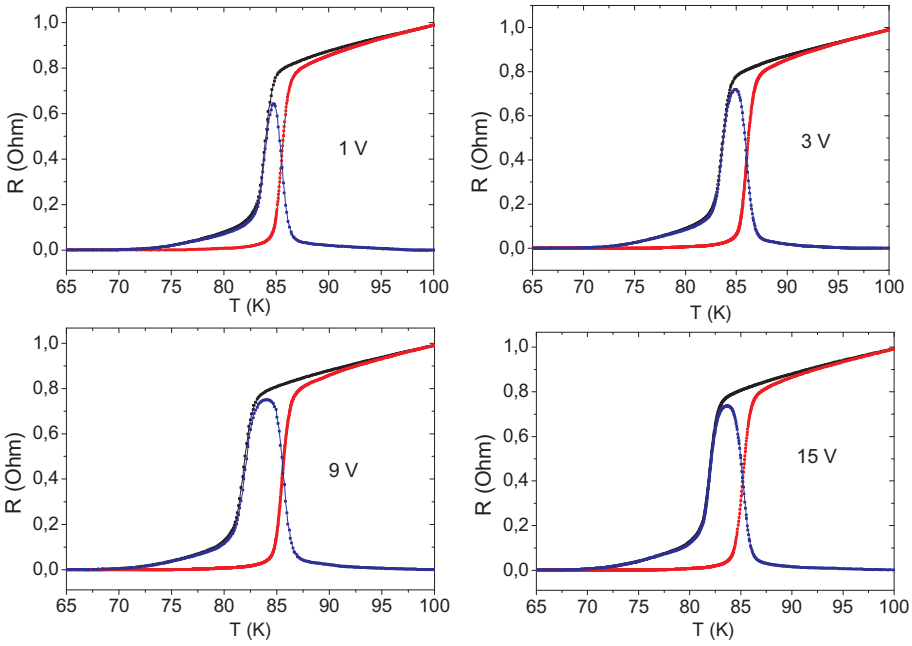

Fig. 9. Temperature dependence of the resistance of YBCO measured between contacts V_1 and V_2 in the vicinity of superconducting transition, for the current flowing through the contacts I_1 and I_3 (black curves), and I_1 and I_2 (red). Curves for four values of load voltage from 1 to 15 V are shown in different subplots. Blue curves are the difference curves between black and red ones. (For interpretation of the references to color in this figure legend, the reader is referred to the web version of this article.)

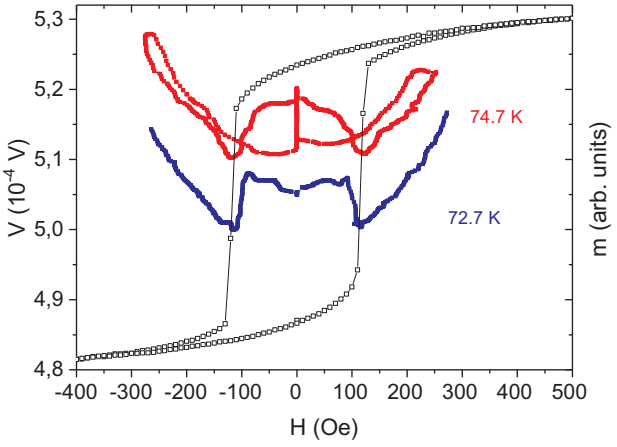

Fig. 10. Magnetic field dependence of the voltage in YBCO in the resistive state (blue and red curves, left axis) at two different temperatures of 72.7 and 74.7 K shown in the plot. Overlapped to this picture is the magnetization loop of LCMO (right axis). Minima of resistance are developed at the coercive fields of LCMO. (For interpretation of the references to color in this figure legend, the reader is referred to the web version of this article.)

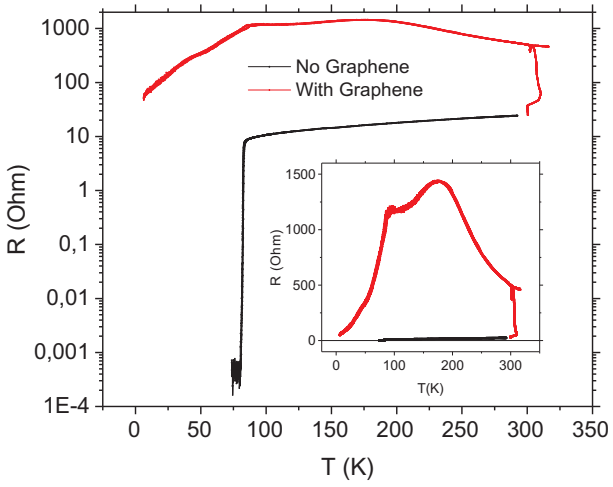

Fig. 11. Temperature dependence of the resistance of YBCO deposited above the LCMO, measured directly during and after the contact with water solution of graphene (red curve), and before the contact (black curve). The axis of resistance is in the logarithmic scale for the main plot, and in the linear scale for the inset. (For interpretation of the references to color in this figure legend, the reader is referred to the web version of this article.)

clearly seen in the plot. When the average magnetization in LCMO is zero at its coercive fields (see magnetization loop shifted and overlapped with the plot), resistance of YBCO develops the minima. Such an experiment justifies the use of the term 'spin injection' in the description of phenomena observed in the transport measurements of the bilayers.

To extend the above activity to a wider range of materials expected to operate at high temperatures, a combination of YBCO and LCMO with graphene was explored. A drop of a water solution containing large number of graphene micro-flakes was set on YBCO surface of YBCO/LCMO bilayer simultaneously measuring its temperature dependence of resistance. The results of this experiment are shown in Fig. 11 by red line. The black line shows R(T) of the same sample before the contact with the graphene solution. Strong increase in resistance is clearly seen in the plot. The resistance of LCMO layer below YBCO was revealed after the contact of the bilayer with the graphene solution, as is more clearly seen in the linear plot in the inset. The position of LCMO resistivity peak in this sample is somewhat lower than optimal 250 K.

This shift of the peak in resistance is not due to an influence of graphene solution on LCMO. Separate measurements on LCMO did not show significant influence on Curie temperature and even resistance of the material. The strong influence on YBCO is associated with the presence of grain boundaries in the material. Both water and graphene are able to affect YBCO along the grain boundaries. Separate experiments on a single-crystalline YBCO bridge without grain boundaries indeed showed the absence of such an influence. This could be useful for hybrid applications of YBCO, LCMO and graphene.

4. Summary

A study of the *in-situ* LCMO film partially covered by the *c*-axis oriented YBCO by electrical transport measurements at a wide range of temperatures has been performed using an array of current and potential leads. Strong influence of LCMO on normal and superconducting

state of YBCO is demonstrated. The origin of unusual peak in resistance appearing below the superconducting transition in *ex-situ* bilayer with *ab*-plane oriented YBCO is clarified. The combination of graphene with YBCO and LCMO was explored indicating vulnerability of YBCO along its grain boundaries.

References

[1] D. Castelvecchi, Quantum cloud goes commercial, Nature 543 (2017) 159.
[2] J. Linder, J.W.A. Robinson, Superconducting spintronics, Nat. Phys. 11 (2015) 307.
[3] Y.-P. Shim, C. Tahan, Semiconductor-inspired design principles for superconducting quantum computing, Nat. Commun. 7 (2016) 11059.
[4] A.K. Geim, K.S. Novoselov, The rise of graphene, Nat. Mater. 6 (2007) 183.
[5] R. Werner, C. Raisch, A. Ruosi, B.A. Davidson, P. Nagel, M. Merz, S. Schuppler, M. Glaser, J. Fujii, T. Chassé, R. Kleiner, D. Koelle, $YBa_2Cu_3O_7/La_{0.7}Ca_{0.3}MnO_3$ bilayers: Interface coupling and electric transport properties, Phys. Rev. B 82 (2010) 224509.
[6] N.C. Yeh, R.P. Vasquez, C.C. Fu, A.V. Samoilov, K. Vakili, Nonequilibrium superconductivity under spin-polarized quasiparticle currents in perovskite ferromagnet-insulator-superconductor heterostructures, Phys. Rev. B 60 (1999) 10522.
[7] P. Mikheenko, M.S. Colclough, C. Severac, R. Chakalov, F. Welhoffer, C.M. Muirhead, Effect of spin-polarized injection on the mixed state of $YBa_2Cu_3O_{7-\delta}$, Appl. Phys. Lett. 78 (2001) 356.
[8] S. Soltan, J. Albrecht, H.-U. Habermeier, Transport properties of LCMO/YBCO hybrid structures, Mater. Sci. Eng. B 144 (2007) 15.
[9] E. Dagotto, T. Hotta, A. Moreo, Colossal magnetoresistace materials: the key role of phase separation, Phys. Rep. 344 (2001) 1.
[10] L.P. Gor'kov, V.Z. Kresin, Mixed-valence manganites: fundamentals and main properties, Phys. Rep. 400 (2004) 149.
[11] P.E. Schiffer, A.P. Ramirez, W. Bao, S.W. Cheong, Low temperature magnetoresistance and the magnetic phase diagram of $La_{1-x}Ca_xMnO_3$, Phys. Rev. Lett. 75 (1995) 3336.
[12] C.M. Fang, G.A. De Wijs, R.A. De Groot, Spin-polarization in half-metals, J. Appl. Phys. 91 (2002) 8340.
[13] S. Soltan, J. Albrecht, H.-U. Habermeier, Spin-polarized quasiparticle injection effects in YBCO thin films, Solid State Commun. 135 (2005) 461.
[14] S. Soltan, Interaction of Superconductivity and Ferromagnetism in YBCO-LCMO Heterostructures, Cuvillier Verlag, Göttingen, 2005.
[15] F. Chen, B. Gorshunov, G. Cristiani, H.-U. Habermeier, M. Dressel, Suppression of superconductivity in YBCO/LCMO superlattices, Solid State Commun. 131 (2004) 295.
[16] A.H. Yonamine, S.A. Fedoseev, D.I. dos Santos, A.V. Pan, Magnetic properties of YBCO/LCMO superlattices with and without STO Interlayers, Adv. Mater. Res. 975 (2014) 101.
[17] A.I. Buzdin, Proximity effects in superconductor-ferromagnet heterostructures, Rev. Mod. Phys. 77 (2005) 935.
[18] H. Yang, S.H. Yang, S. Takahashi, S. Maekawa, S.S. Parkin, Extremely long quasiparticle spin lifetimes in superconducting aluminium using MgO tunnel spin injectors, Nat. mater. 9 (2010) 586.
[19] N. Poli, J. Morten, M. Urech, A. Brataas, D.B. Haviland, V. Korenivski, Spin injection and relaxation in a mesoscopic superconductor, Phys. Rev. Lett. 100 (2008) 1136601.
[20] T. Wakamura, N. Hasegawa, K. Ohnishi, Y. Niimi, Y. Otani, Spin injection into a superconductor with strong spin-orbit coupling, Phys. Rev. Lett. 112 (2004) 036602.
[21] C.H.L. Quay, D. Chevallier, C. Bena, M. Aprili, Spin imbalance and spin-charge separation in a mesoscopic superconductor, Nat. Phys. 9 (2013) 84.
[22] A.S. Fjellvåg, T.B. Hjelmeland, H.J. Mollatt, T. Qureishy, P. Mikheenko, Interplay between spin polarization and superconductivity in an ex-situ bilayer $La_{0.67}Ca_{0.33}MnO_3$ – $YB_a2C_u3_{O7-}x$, IEEE Xplore Digital Library 8190363 (2017).
[23] P. Mikheenko, Graphene-assisted transport measurements of biological samples, IEEE Xplore Digital Library 7757272 (2016).
[24] P. Mikheenko, Possible superconductivity in the brain, J. Supercond. Nov. Magn. (2018), https://doi.org/10.1007/s10948-018-4965-4.
[25] H. Zhang, N. Gauquelin, G.A. Botton, J.Y.T. Wei, Attenuation of superconductivity in manganite/cuprate heterostructures by epitaxially-induced CuO intergrowths, Appl. Phys. Lett. 103 (2013) 052606.